Earth Surface Processes and Landforms
Earth Surf. Process. Landforms **31**, 1413–1423 (2006)
Published online 17 May 2006 in Wiley InterScience
(www.interscience.wiley.com) **DOI:** 10.1002/esp.1341

Feature based image processing methods applied to bathymetric measurements from airborne remote sensing in fluvial environments

Patrice E. Carbonneau,[1]* Stuart N. Lane[2] and Normand Bergeron[1]
[1] *INRS Centre Eau, Terre et Environnement, 490 Rue de la Couronne, Québec, Canada G1K 9A9*
[2] *Department of Geography, University of Durham, Science Site, South Road, Durham DH1 3LE, UK*

**Correspondence to: Patrice E. Carbonneau, Department of Geography, University of Durham, Science Site, South Road, Durham DH1 3LE, UK.*
E-mail: patrice.carbonneau@dur.ac.uk

Received 11 May 2005;
Revised 29 September 2005;
Accepted 10 October 2005

Abstract

Bathymetric maps produced from remotely sensed imagery are increasingly common. However, when this method is applied to fluvial environments, changing scenes and illumination variations severely hinder the application of well established empirical calibration methods used to obtain predictive depth–colour relationships. In this paper, illumination variations are corrected with feature based image processing, which is used to identify areas in an image with a near-zero water depth. This information can then be included in the depth–colour calibration process, which results in an improved prediction quality. The end product is an automated bathymetric mapping method capable of a 4 m^2 spatial resolution with a precision of ±15 cm, which allows for a more widespread application of bathymetric mapping.

Keywords: bathymetry; image processing; remote sensing; rivers

Introduction and theoretical considerations

The use of remotely sensed pixel colour to map water depth in fluvial environments by the application of calibrated depth–colour relationships is well documented. Multispectral (Lyon *et al*., 1992; Winterbottom and Gilvear, 1997; Marcus, 2002; Whited *et al*., 2002; Marcus *et al*., 2003), colour (Westaway *et al*., 2003) and greyscale (Winterbottom and Gilvear, 1997) imagery have all been used for bathymetric mapping. For all three image types, the bathymetric mapping methods rely on the same theoretical basis. The physical principle underlying the measurement of flow depth from brightness levels in imagery is the Beer–Lambert law, which describes the absorption effect as light passes through transparent media. If a beam of light with an incoming intensity I_{in} passes through a transparent medium of thickness x, the remaining outgoing intensity I_{out} can be written as (Serway, 1983)

$$I_{out} = I_{in}\, e^{-cx} \tag{1}$$

where c is the rate of absorption of the medium, which varies according to properties of the medium, such as turbidity, and the frequency of the incident light. The intensity of light therefore decreases as an exponential function of the distance passed through the medium. In the case of digital imagery, the light intensity is captured as discreet brightness levels. The term I_{out} will therefore be the final observed brightness levels in the image and the term I_{in} will be the initial brightness of the bed before the passage of light through the water column. This explains why shallow submerged areas have a brighter colour than deep submerged areas.

In the above, bathymetric mapping relies on the determination of the constant c and the initial brightness I_{in}. The calibration procedures for the determination of these parameters can be divided into two groups. First, empirical methods have used geolocated field measurements of depth in a regression model to establish depth as a function of colour (Winterbottom and Gilvear, 1997; Marcus, 2002; Westaway *et al*., 2003; Fonstad and Marcus, 2005). Second, physical methods have used water sampling to predict the absorption of light by the water column (Lyon *et al*., 1992). The empirical method is the most cited in published work and will be the basis for the work in this paper.

The success of calibration methods and the quality of the predictions are most affected by the type of imagery that has been used. Generally, studies using multispectral imagery report better prediction quality. Multispectral imagery allows for the use additional image bands to classify bottom types (i.e. sand, gravel, algae) and thus construct depth–colour relationships for each bottom type, which lead to improved results. For example, Winterbottom and Gilvear compared results of multispectral and grey scale imagery (Winterbottom and Gilvear, 1997). They obtained a model with $R^2 = 0{\cdot}67$ in the multispectral case and $R^2 = 0{\cdot}55$ in the greyscale case. Other researchers obtained even better results from multispectral data, the highest reported value being a prediction quality R^2 of 0·95 (Lyon *et al*., 1992). Multispectral imagery is therefore normally considered as the method of choice for bathymetric measurements. However, standard colour imagery still retains certain advantages over multispectral imagery. Recent modelling by Legleiter *et al*. (2004) suggests that band ratios calculated from colour imagery can be as effective as multispectral imagery. Additionally, the cost of a multispectral image survey is still much greater than that of a standard colour equivalent (Roberts and Anderson, 1999). Furthermore, standard colour imagery can attain centimetre scale resolution whilst multispectral imaging sensors are still generally limited to metre scale resolution. Carbonneau *et al*. (2005) and Carbonneau *et al*. (2004) have shown that high resolution colour imagery can be used to carry out fully automated measurements of grain size in dry exposed areas. If reliable depth estimates could be made with the images used to measure grain size, a very powerful tool capable of automated measurements of both depth and grain size could be developed. Such a remote sensing approach to river characterization could have a major impact on future research in all fields interested in fluvial environments.

The use of high resolution imagery for automated depth measurement has specific difficulties. In particular, if centimetre resolution airborne imagery is collected at the catchment scale, this necessarily implies that a very large number of photographs, hundreds to thousands, will be required to cover the whole study area. In such cases, the use of digital images to measure light intensity value can be problematic. As described by Fonstad and Marcus (2005), when applying bathymetric models to imagery, it is necessary to measure the light intensity with the digital number of each image pixel. Therefore, photography principles such as aperture and exposure times should be considered, since these factors control the conversion of actual light intensity in the field to digital image numbers. Of particular importance is the case where camera exposure and aperture settings are variable within the image data set since the conversion from light intensity to digital numbers will vary accordingly. In the case of large image data sets, this variability can be problematic since identical lighting conditions in the field may not be represented by identical digital image numbers in the imagery. There is a significant body of literature describing the physics of bathymetric mapping (Lyon *et al*., 1992; Lyon and Hutchinson, 1995; Legleiter *et al*., 2004). However, these methods all assume that identical light conditions in the field will produce identical image brightness levels. Therefore, the issues of variable camera apertures and exposures leading to variable image illumination must be addressed separately. This specific problem has not been discussed in the literature owing to the recent availability of high resolution image data sets comprised of thousands of images. The aim of this paper is therefore to develop a bathymetric mapping method that can operate with thousands of images and that incorporates a correction factor for variable camera conditions.

Approach

Since achieving a perfectly constant camera exposure and aperture over very large areas is not possible due to inevitable changes in weather conditions and scenery, the most practical solution to this problem is correcting the brightness levels in the imagery with an image processing application. The most obvious solution to the problem is to use the standard image processing method of histogram matching to correct the base illumination differences (Castleman, 1996). Histogram matching operates by comparing the initial image histogram that is to be corrected to a reference histogram. The goal of the process is to redistribute the initial histogram bin values in order to reshape the initial histogram to the shape of the reference histogram. This process differs significantly from linear histogram stretching in that a linear scaling factor is applied to both the brightness values of the histogram bins and the number of counts within each bin. For large image data sets, this method can be implemented in two ways. The first option is to match all the image histograms to a reference histogram. The second is to match each image histogram to that of its neighbour in the data set. The difficulty with the first option is the determination of the reference histogram. If the reference histogram and the image histogram differ too much, the results will be poor. In the case of high resolution imagery in fluvial environments, changes in the image scene will lead to histograms having different shapes independently from the level of base illumination. For example, Figure 1 shows image histograms with their associated images. The images in Figure 1(A) and (B) are separated by 80 m and taken at a 1 s interval. Despite this close proximity in space and time, the images have important differences due to the rapidly changing scenery. In this case, a dry exposed bar has developed along the flight path in Figure 1(B). As a result of the appearance of this dry bar which has a higher brightness level, the camera exposure was automatically reduced to compensate. The consequence is that Figure 1(B)

DOI: 10.1002/esp

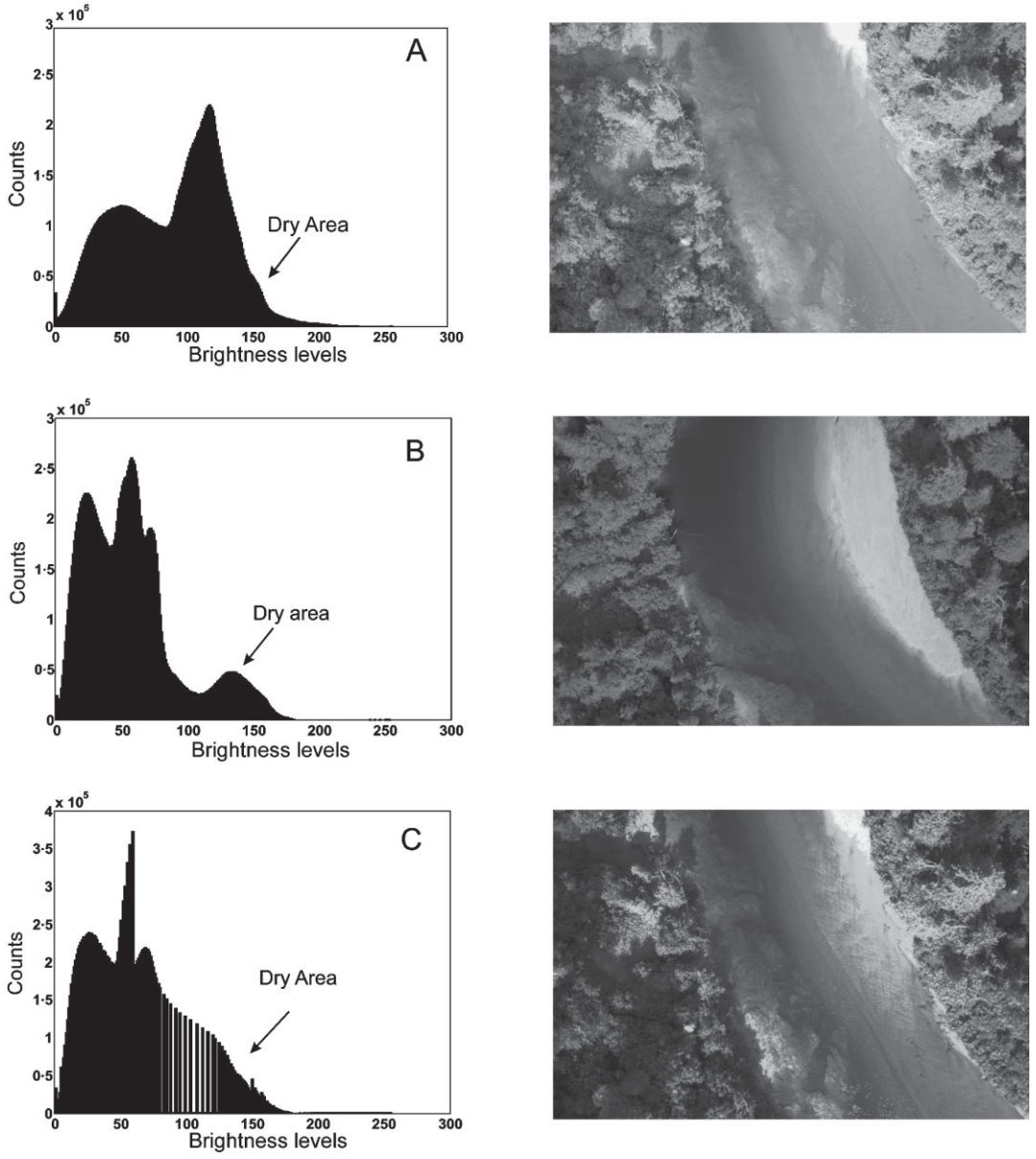

Figure 1. Example of histogram matching failure. (A) Histogram and image having very little dry area. (B) Histogram and image with lower base illumination and more dry areas. (C) Result of matching histogram A to histogram B.

is darker thus showing a typical example of the type of problem this work seeks to correct. This change in scenery and illumination has important consequences on the image histogram that need to be considered before applying a histogram matching correction. Dry exposed areas have higher brightness levels than other areas and their spatial extent in Figure 1(A) is much lower than that in Figure 1(B). Therefore, these scenes should have different histograms and scaling them on to a single histogram is unlikely to be meaningful. For example, Figure 1(C) shows the results of using the histogram in Figure 1(B) as a reference histogram for application to Figure 1(A). The resulting histogram and image clearly show the failure of the matching process. There has been creation of an artificial dry area mode at brightness levels of 150. In the image, an area of the wetted perimeter has been significantly altered as a result of the artificial dry area peak in Figure 1(B). This has created a false dry bank. It is therefore clear that, given the variety of histogram shapes that can occur in scenes of fluvial environments within the same river, selection of a universal reference histogram is highly problematic.

DOI: 10.1002/esp

In the case where neighbouring images have similar histograms, the second histogram matching option, which matches neighbouring histograms, gives visually pleasing results. Since it smoothes out local differences in illumination in neighbouring images, local visual inspection of the results will show a uniform base illumination. However, at a larger scale, gradual and slowly varying illumination differences can persist, which can cause errors in bathymetric mapping. Therefore, the second option of histogram matching does not seem more appropriate if depth measurements are required from the image data set. Additional research is therefore required to adapt existing depth–colour calibration methods to the specific problems associated with large image data sets in fluvial environments.

An alternative form of illumination correction can be developed by understanding the physics of the process. Equation (1) shows that two parameters must be calibrated for successful bathymetric mapping: the constant c and the incident illumination I_{in}. Since the value of c, the rate of light absorption, is a function of water turbidity and light frequency, it can be reasonably assumed that c is constant for the whole system. In practice, allowing c to vary is one way of compensating for variations in illumination (i.e., c can be varied to give an empirically justifiable form of Equation (1)). However, this is not a physically correct approach. Here, we focus attention on the incident light intensity term I_{in}. Since brightness decreases with increasing depth, it can be reasoned that the initial brightness levels can be obtained if one conceptually removes the water medium to look at the brightness level of the bed. In such a case, one is left with *wetted* clasts that are *not* submerged. If the spectral properties of such clasts can be identified, and if we assume that they are constant for the whole system, a semi-empirical bathymetric mapping approach should be possible that automatically corrects for illumination conditions. The first step is to identify unsubmerged wetted clasts in an image with automated feature based image processing. Such clasts can be found in an image by locating the wet/dry interface using image classification. Therefore a good quality image classification will be required to insure that the wet/dry interface can be located. Second, the brightness levels of these clasts can be used as the I_{in} term in Equation (1). Third, an empirical approach can be used to calibrate the rate of absorption constant c.

Methods

Airborne digital imagery acquisition

The work discussed in this paper uses a set of high resolution airborne imagery. Data were obtained for the main branch of a gravel bed salmon river in Quebec, Canada: the Sainte-Marguerite river. The survey covered the full 80 km of the main branch where the channel width varies from a few metres at the headwaters to approximately 80 m at the mouth. In August 2002, a helicopter survey was carried out during the summer period of low flow. The XEOS™ system, developed by GENIVAR inc., was used to obtain plan view digital imagery of the entire 80 km study area. The helicopter survey was carried out at an altitude above the bed of 155 m in order to obtain digital imagery with a ground resolution of 3 cm (1:350 scale). Image format was 3008 pixels × 1960 pixels in the standard visible bands of red, green and blue. Images were collected at 60 per cent overlap to allow for photogrammetric work to be carried out in the future. Two days were required to complete the surveys yielding 4184 images. Flights were carried out between 10 am and 3 pm with weather conditions being generally cloudy and dry with sunny spells. Figure 2 shows a greyscale example of the resulting imagery. Since the images have 60 per cent overlap, full coverage of the 80 km study reach can still be achieved by taking every other image. Therefore 2092 images were used in this study.

Field data

Calibration and validation data for the depth measurement method were collected with a Leica 500 RTK GPS capable of 3–5 cm precision in both horizontal and vertical directions. Since no tributary brings a major input of suspended sediment that could alter the rate of absorption term, calibration measurements were concentrated on a reach of approximately 250 m length. First, water surface measurements were taken along the study reach at approximately 5 m intervals in order to model the elevation of the water surface. This yielded 50 points, which were input into a regression plane to define the water surface elevation. Second, 1500 GPS measurements were taken in the wadable area of the flow. The resulting elevations were subtracted from the water surface to obtain water depth. 500 of these points were set aside for validation purposes and 1000 were used in the model calibration.

Each depth obtained from a GPS coordinate was related to an image location by georeferencing the images covering the study site. The 250 m study site was covered by four images. Within these images, a total of 24 control points were laid out before the image acquisition flight. These control points were surveyed with the GPS and georeferenced with ArcMap software from ESRI. The horizontal precision of the georeferencing was estimated at

DOI: 10.1002/esp

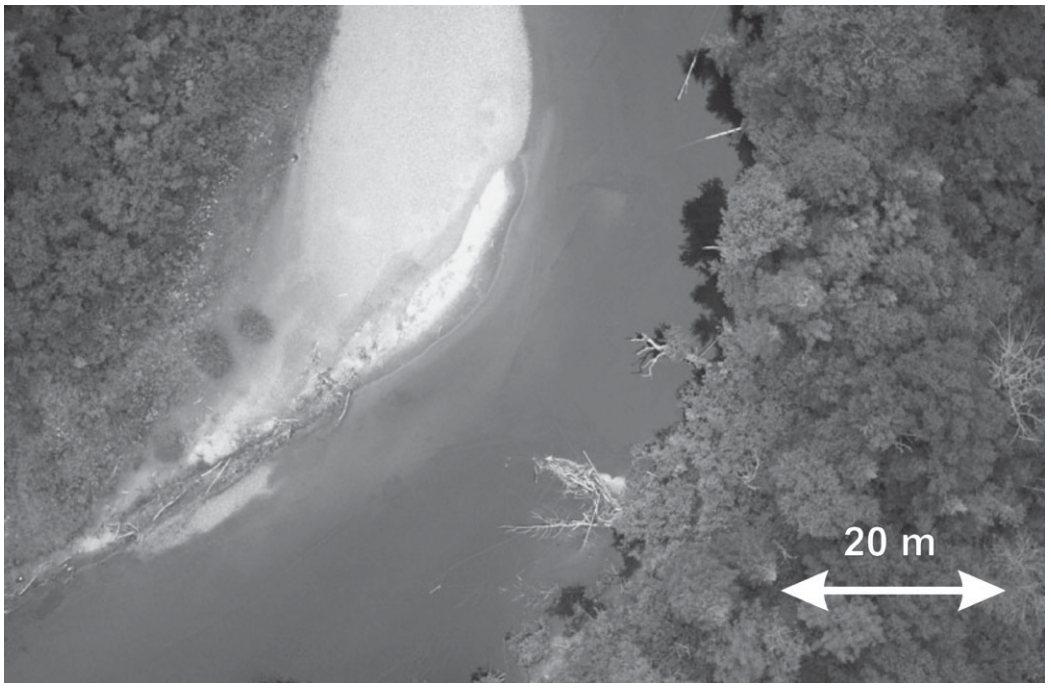

Figure 2. Sample image from the St-Marguerite river study site located at 48·38° N 70·20° W.

±27·8 cm RMS. The georeferencing process allowed for the measured depth to be related to exact image coordinates so allowing the modelling process to begin.

Image classification

The automated image classification algorithm discussed by Carbonneau *et al*. (2004), capable of identifying dry areas in an image, was expanded to perform automated classifications of vegetated areas and wetted areas. The accuracy of the classification was estimated by taking 10 images and comparing the automated classification with a manual classification. Image pixels were then labelled as 1 for a correct classification and 0 for a false classification. This resulted in approximately 80 per cent of pixels being correctly classified. Given that the identification of the wet/dry interface is pivotal to the entire correction procedure, a higher quality classification was required. Therefore, a semi-automated interface was designed in the MATLAB environment to allow for a rapid and efficient editing process. This semi-automated interface was designed to manage repetitive tasks such as image uploading and saving while taking advantage of human pattern recognition skills to identify classification errors. The interface functions by displaying both the image and the raw classification image. The user can then rapidly correct classification errors by drawing directly on the image. With this highly efficient interface a single user can edit approximately 200 image classifications per day. Therefore approximately 2 weeks were required to fully edit the 2092 image classifications.

Rate of absorption calibration

Equation (1) was used as the basic model for calibrating the depth–colour relationships. Since no important source of suspended sediment occurs along the study area, it was assumed that the rate of absorption is constant for the whole data set. The rate can be calibrated with the field data by plotting the calibration data on semilogarithmic axes and applying a linear regression model. However, some practical considerations must be given before assigning a brightness value to a depth measurement. The first factor that must be considered is colour. Since rate of absorption is a function of wavelength (i.e. colour), the optimal colour, or colours, must be selected among the three available colour bands. Winterbottom and Gilvear (1997) investigated bottom reflectance, the opposite of absorption, as a function of water depth and wavelength. If we consider the three wavelengths of ≈600 nm for red, ≈500 nm for green and ≈400 nm for blue, the results of Winterbottom and Gilvear show that, for shallow environments, the red colour band

DOI: 10.1002/esp

is the most sensitive to depth variations, with the green band having some sensitivity and the blue band having poor sensitivity to depth variations. Legleiter *et al*. (2004) have also found that the red colour band is most suitable for shallow environments. Visual examination of our imagery clearly confirmed these findings, showing that the red band is most sensitive to depth change. Furthermore, examination of the blue band revealed that it was insensitive to depth variations. It was therefore decided to proceed with the red band in the analysis.

The second practical consideration that needs to be addressed is bed material colour variations. Since the model assumes that brightness is a function of depth, local variations in bed material colour and shading are not accounted for and thus introduce noise to the model. For this reason, single pixel brightness values are not used and some form of local averaging within the wetted perimeter is employed. However, no guidelines exist for the selection of the appropriate window size for averaging. It was therefore decided to test the effect of increasing the averaging area on the final model quality. Therefore, depth–colour calibration relationships were examined for five averaging areas: 1×1 pixel (i.e. no averaging), 3×3 pixels, 9×9 pixels, 33×33 pixels and finally 66×66 pixels. These averaging windows were only applied to the wetted perimeter. In each case, the image classification was used to exclude all pixels that were not in the wetted perimeter. This was done to insure that no dry exposed bed brightness values were erroneously used in the calibration relationship. Given the exclusion of non-wetted areas, window sizes beyond 66×66 pixels were impractical since the size of the window becomes comparable to the width of the channel at the headwaters. Therefore, window sizes larger than 66×66 pixels were considered as too large to adequately capture depth variations and were excluded from the analysis.

Once the optimal averaging window is identified, an initial calibration model was constructed by regressing observed depth versus averaged pixel brightness, without accounting for the brightness levels of unsubmerged wetted clasts, thus yielding a model in the form of Equation (1). It was validated using the depth measurements that were set aside for this purpose. This initial model will then be used to assess the effectiveness of the unsubmerged wetted clast colour calibration.

Unsubmerged wetted clast colour calibration

The empirical process used to calibrate the colour of an unsubmerged wetted clast was replaced with a feature based image processing approach. The process starts by using the classification data to identify two distinct features in the image: the dry areas and the wetted areas. Edge detection with a standard Sobel operator (Castleman, 1996; Richards and Xuiping, 1999) applied to these two areas allows for the identification of the wet/dry interface in the image. It is then assumed that the pixels in the wetted perimeter that are immediately adjacent to the wet/dry interface are at near-zero depth and therefore represent the wetted clast colour in the absence of inundation. The average value of these pixels is then taken as the constant, I_{in}, in Equation (1). To obtain a valid calibration, field calibration points located in different images need to be plotted in the same regression model. Therefore, the obtained value for I_{in} is used to calculate the magnitude of a linear histogram shift applied to each image and designed to bring the value of I_{in} to a standardized 128. This value was arbitrarily chosen to be in the centre of the 0–255 brightness range. This is in effect an illumination correction. The final calibration model was therefore established from corrected images where the unsubmerged wetted clast colour has been used to perform an illumination correction.

Once this image processing step is complete, another experimental analysis of quality versus averaging window size was carried out in order to fully assess the effect of this new calibration procedure. The window sizes used in this test were again 1×1, 3×3, 9×9, 33×33, 66×66.

Bathymetric map production

If the results of the calibration give reliable results for c, bathymetric maps can be produced. These maps were produced by isolating the shallow wetted area with the image classification. Then, a smoothing window, whose dimensions were determined experimentally, is applied to reduce local noise effects. Feature based image processing was applied to determine the value of I_{in}. Finally Equation (1) was used with the calibrated value for c, $I_{in} = 128$, and the rescaled image data, to produce the final bathymetric maps. Since 2092 images must be processed, data storage is an issue. It was decided to store the depth maps as jpeg eight-bit (0–255) greyscale images and therefore benefit from the jpeg compression. To conform to the eight-bit format, the calculated depths were converted to centimetres. This allows for a range of depths of 0–255 cm, which is appropriate for shallow fluvial environments. The output of the bathymetric maps was limited to depths where the bed is still visible. In the case of the St-Marguerite river, this is approximately 1·5 m. Therefore, any values found to be deeper than 150 cm were set to 255 cm. Points in the resulting bathymetric maps with a value of 255 should therefore be considered to be deeper than 150 cm.

DOI: 10.1002/esp

Table I. Regression quality of depth vs brightness as a function of the size of the averaging window with and without illumination corrections

Window size	R^2 (without illumination correction)	R^2 (with illumination correction)
1 × 1	0·03	0·14
3 × 3	0·05	0·15
9 × 9	0·08	0·19
33 × 33	0·14	0·32
66 × 66	0·21	0·49

Results

Table I shows the results of the averaging area testing, which was conducted for both the conventional and uncorrected cases. It can be seen that better results are obtained with the biggest averaging area, 66 × 66. This corresponds to 2 m × 2 m on the ground, and is used for the development and application of the calibration results.

Conventional calibration approach

Figure 3(A) shows the associated regression plot for the 66 × 66 window case. Multiple parallel trends can be seen in this figure, which explains the poor R^2 results in Table I. In Figure 3, the data from each individual image was plotted with different symbols, which clearly shows that each trend can be associated with a separate image. If we attempt to calibrate this uncorrected data, calibration Equation (1) takes the following form:

$$I_{\text{red}} = 109{\cdot}5\ \text{e}^{-0{\cdot}596H} \tag{2}$$

where I_{red} is the brightness level in the red band and H is the depth. In Equation (2), the incident light value (I_{in}) is 109·5 and it should be noted that this value was obtained as the intercept of the regression. If Equation (2) is applied to the imagery and predicted depths are assessed using the validation data (Figure 3(B)), the presence of multiple trends causes a very large scatter and the estimates of depth are biased to −12 mm and have a precision of ±367 mm.

Illumination-corrected approach

In relation to sensitivity to averaging window size, illumination correction results in a substantial increase in model quality (Table I). Figure 4(A) shows the associated regression plot for the 66 × 66 pixel case. It can be seen that this correction has collapsed the multiple trends shown in Figure 3(A) on to a single relationship. The optimal depth–colour relationship obtained after the standardization of the unsubmerged wetted clast colour was

$$I_{\text{red}} = 128\ \text{e}^{-0{\cdot}387H} \tag{3}$$

where I_{red} is the brightness level in the red band and H is the depth. In Equation (3), the incident light value (I_{in}) is 128. In this case, this value was preset by the illumination correction procedure. Once the optimal model has been established, the 500 points set aside for validation were used to assess the quality of the depth predictions. Figure 4(B) shows the results. It can be seen that the addition of the unsubmerged clast calibration has considerably reduced the scatter. The resulting bias has been reduced from −12 mm to −8 mm, and the precision improved from ±367 mm to ±155 mm. When taken with the improvement in R^2 from 0·21 to 0·49, this suggests that the correction method is an excellent development in allowing application of the semi-empirical approach in (1) to multiple imagery.

Bathymetric maps

This optimal model can then be used to produce bathymetric maps for the whole image set. The value for the rate of absorption is taken from Equation (3) as being equal to 0·387 and the feature based image processing method is applied to each image to determine the value of the initial light intensity, I_{in}. The processing time needed to produce

DOI: 10.1002/esp

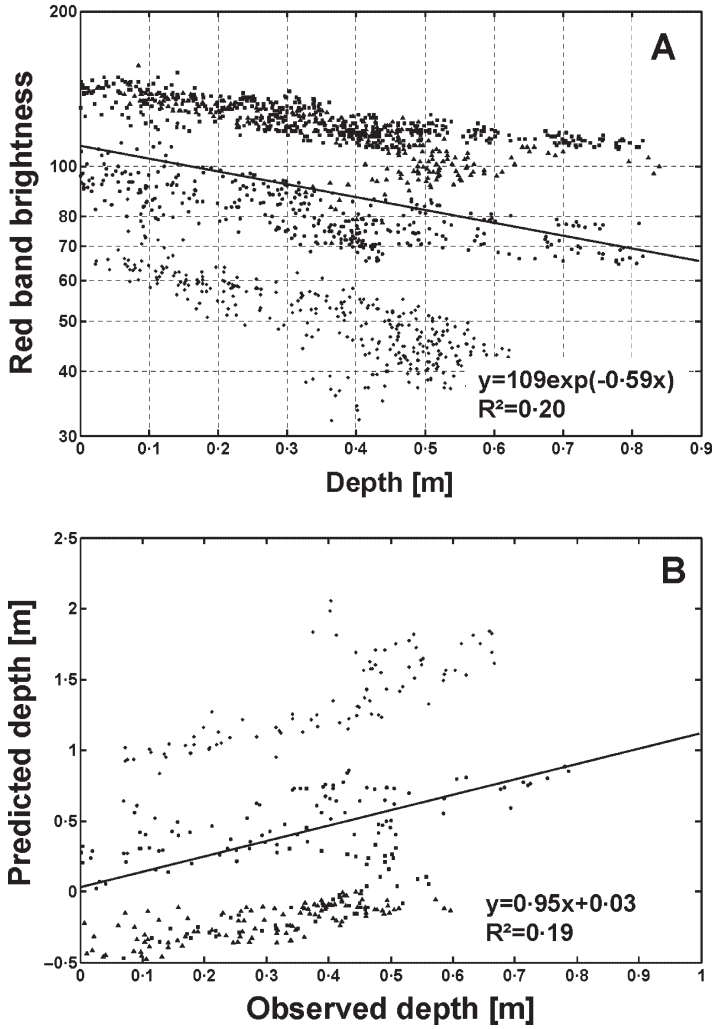

Figure 3. Depth–colour modelling without calibration of the unsubmerged wetted cast colour. Four distinct symbols are used to differentiate between the four different source images. (A) Calibration model for a 66 × 66 averaging window. (B) Validation of the model shown in (A).

the bathymetric maps for the set of 2092 images, excluding the time require to edit the image classifications, was approximately 24 hours on a PC computer clocked at 3 GHz. Figure 5 shows an example of a bathymetric map.

Discussion

Comparisons of Figures 3(B) and 4(B) shows an improvement in prediction quality. The scatter remaining in Figure 4(B) can partially be attributed to resolution differences between the bathymetric map data and the GPS validation data collected in the field. Since the field data was collected with a centimetre precision GPS system, the depth measurements were highly localized and did not account for any depth variability in the area adjacent to the sample. The final resolution of the bathymetric mapping method was 4 m^2; therefore, the difference in resolutions between field data and method output will induce additional variability in the validation results. Better results could be achieved in the future if the validation data and the outputs have similar spatial resolutions.

Two additional sources of error should be mentioned for their potential impact on basin scale depth measurements. First, as stated earlier, the process described in this paper assumes that the rate of absorption constant c is constant throughout the system. One notable exception can be found to this rule: surface turbulence such as white water rapids.

DOI: 10.1002/esp

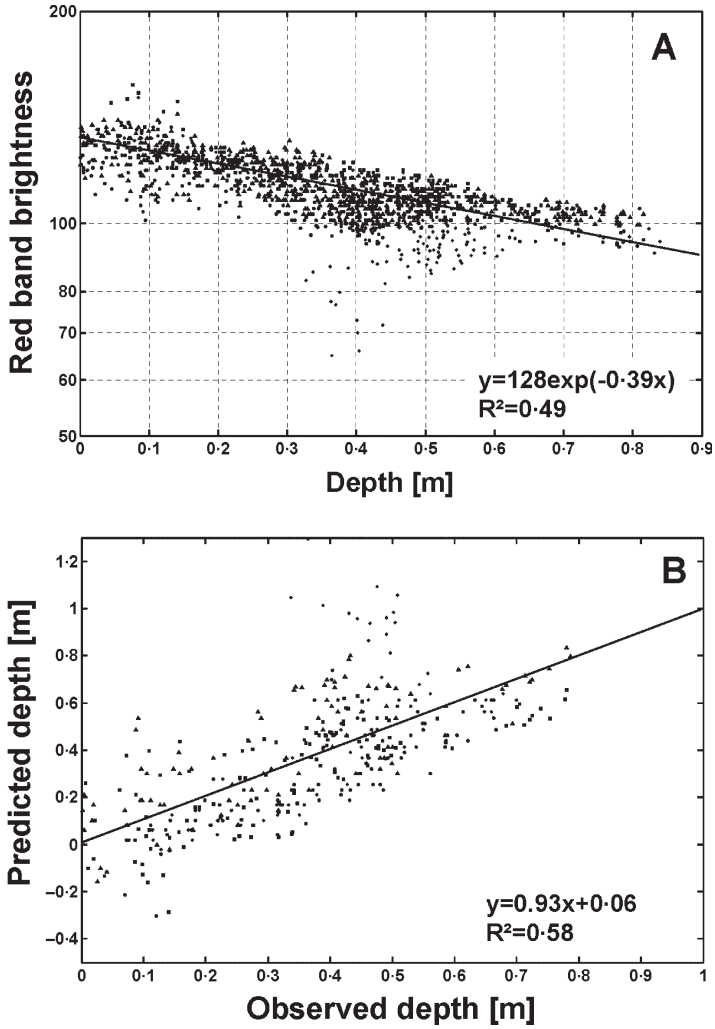

Figure 4. Depth–colour modelling with calibration of the unsubmerged wetted cast colour. Four distinct symbols are used to differentiate between the four different source images. (A) Calibration model for a 66×66 averaging window. (B) Validation of the model shown in (A).

In such cases, the water surface essentially becomes opaque and thus all information concerning the riverbed is lost. An examination of the data set used in this paper suggests that white water occupies less than 2 per cent of the entire wetted surface. Therefore, the authors believe that these areas can simply be removed from the analysis without causing a significant loss of information. Another source of error that should be considered is bank shading. Depending on the solar elevation at the time of the flight and the orientation of the channel, banks can be more or less shaded. This has an impact on bathymetric measurements, since the darkened shaded areas will falsely be interpreted as being deeper. Operational procedures for aerial surveys typically restrain the minimum solar elevation angle to 35–45°. This limits potential shading effects. However, it should be noted that heavily vegetated banks do cause additional error, which will probably always be part of image based bathymetric mapping in fluvial environments.

Despite the remaining error, the overall precision of the method went from ±367 mm to ±155 mm, a considerable improvement. In addition to these gains in terms of precision, another noticeable improvement can be seen in the near elimination of negative depth predictions. In cases where the brightness levels are higher than the estimated initial brightness (the I_{in} term in Equation (1)), the depth will be predicted as being negative. If the conventional calibration model is used, the poor quality of the calibrated value for the I_{in} term of Equation (1) will lead to a high number of negative depth predictions as seen in Figure 3(B). However, when the I_{in} term is directly calibrated, the number of negative depth predictions is greatly reduced. Some negative predictions remain because the process identifies the

DOI: 10.1002/esp

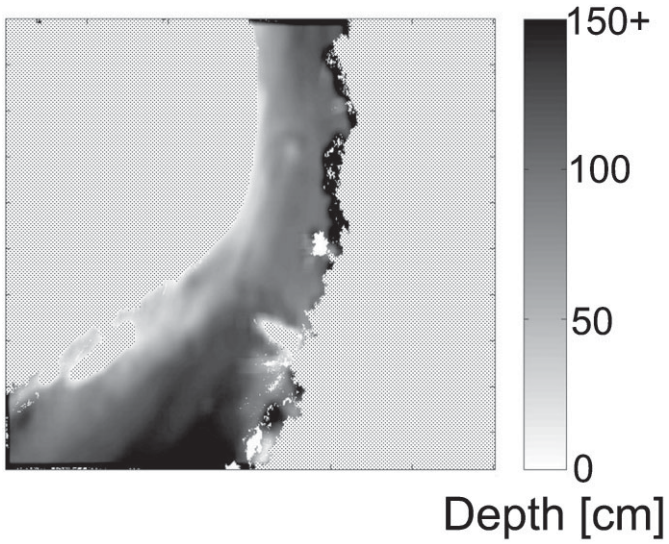

Figure 5. Bathymetric map obtained from the application of Equation (3) to the wetted area of Figure 2.

mean value of unsubmerged wetted clasts and thus variance around the mean may lead to negative depth predictions. However, Figure 4(B) shows that this effect is infrequent, and the low bias value of −8 mm supports this observation. Furthermore, examination of Figure 3(B) shows certain predicted depth values in the vicinity of 1·5 m corresponding to observed depths in the vicinity of 1 m. These values are serious overestimations of depth. Figure 4(B) shows that these overestimations of depth have been eliminated by the illumination correction procedure.

Conclusion

The depth mapping results presented here are less precise than field surveys carried out with GPS or echo sounding equipment. However, if the results of the entire survey are considered, the combination of scale and resolution is unprecedented. Each depth measurement is valid in a 66×66 pixel area, i.e. 4 m^2, corresponding to the smoothing window. The image classification information can be used to measure the total wetted area in the 2092 image survey as 2·3 km^2. This means that we have 589 296 effective depth measurements regularly spaced along both streamwise and cross-stream directions of the channel. Such high resolution and large scale data coverage offsets the lower precision when compared to labour intensive field measurements. Therefore, such an application of feature based image processing to the calibration of depth–colour models, never reported in the literature, should prove useful to other studies seeking to apply remote sensing in fluvial environments and to extract the largest possible amount of information from the imagery.

Acknowledgements

This work was a part of the GEOSALAR project, which is funded by the GEOIDE networks of centres of excellence. This work receives additional funding from the NATEQ postdoctoral scholarship programme and is a contribution to the programme of the Centre Interuniversitaire de Recherche sur le Saumon Atlantique (CIRSA).

References

Carbonneau PE., Bergeron NE, Lane SN. 2005. Automated grain size measurements from airborne remote sensing for long profile measurements of fluvial grain sizes. *Water Resources Research* **41**: W11426 doi: 10.1029/2005WR003994.

Carbonneau PE, Lane SN, Bergeron NE. 2004. Catchment-scale mapping of surface grain size in gravel-bed rivers using airborne digital imagery. *Water Resources Research* **40**: 7.

Castleman KR. 1996. *Digital Image Processing*. Prentice-Hall: Erplewood Cliffs, NJ.

Fonstad MA, Marcus WA. 2005. Remote sensing of stream depths with hydraulically assisted bathymetry (HAB) models. *Geomorphology* **72**(4): 320–329.

Legleiter CJ, Roberts DA, Marcus WA, Fonstad MA. 2004. Passive remote sensing of river channel morphology and in-stream habitat: physical basis and feasibility. *Remote Sensing of Environment* **93**: 493–510.

Lyon JG, Hutchinson WS. 1995. Application of a radiometric model for evaluation of water depths and verification of results with airborne scanner data. *Photogrammetric Engineering and Remote Sensing* **61**: 161–166.

Lyon JG, Lunetta RS, Williams DC. 1992. Airborne multispectral scanner data for evaluating bottom sediment types and water depths of the St. Marys river, Michigan. *Photogrammetric Engineering and Remote Sensing* **58**: 951–956.

Marcus WA. 2002. Mapping of stream microhabitats with high spatial resolution hyperspectral imagery. *Journal of Geographical Systems* **4**: 113–126.

Marcus WA, Legleiter CJ, Aspinall RJ, Boardman JW, Crabtree RL. 2003. High spatial resolution hyperspectral mapping of in-stream habitats, depths, and woody debris in mountain streams. *Geomorphology* **55**: 363–380.

Richards JA, Xiuping J. 1999. *Remote Sensing Digital Image Analysis*, *an Introduction*, 3rd edn. Springer: Berlin, Heidelberg: New York.

Roberts ACB, Anderson JM. 1999. Shallow water bathymetry using integrated airborne multi-spectral remote sensing. *International Journal of Remote Sensing* **20**(3): 497–510.

Serway RA. 1983. *Physics for Scientists and Engineers*. CBS; 132–133.

Westaway RM, Lane SN, Hicks DM. 2003. Remote survey of large-scale braided rivers using digital photogrammetry and image analysis. *International Journal of Remote Sensing* **24**: 795–816.

Whited D, Stanford JA, Kimball JS. 2002. Application of airborne multispectral digital imagery to quantify riverine habitats at different base flows. *River Research and Applications* **18**: 583–594.

Winterbottom SJ, Gilvear DJ. 1997. Quantification of channel bed morphology in gravel-bed rivers using airborne multispectral imagery and aerial photography. *Regulated Rivers: Research and Management* **13**: 489–499.

DOI: 10.1002/esp